Astronomy Reports, Vol. 47, No. 3, 2003, pp. 214–231. Translated from Astronomicheskiĭ Zhurnal, Vol. 80, No. 3, 2003, pp. 239–257.

Interpretation of Light Curves of the Cataclysmic Variable OY Car in a Model with Shockless Interaction between a Gaseous Stream and the Disk

T. S. Khruzina[1], A. M. Cherepashchuk[1], D. V. Bisikalo[2], A. A. Boyarchuk[2], and O. A. Kuznetsov[3]

[1] *Sternberg Astronomical Institute, Universitetskiĭ pr. 13, Moscow, 119899 Russia*

[2] *Institute of Astronomy, Russian Academy of Sciences, ul. Pyatnitskaya 48, Moscow, 109017 Russia*

[3] *Keldysh Institute of Applied Mathematics, Russian Academy of Sciences, Miusskaya pl. 4, Moscow, 125047 Russia*

Received June 22, 2002; in final form, August 21, 2002

Abstract—To determine the parameters of the accretion disk and shock-wave region responsible for the formation of the orbital peak in the light curve of the binary system OY Car (an SU UMa-type variable), we have analyzed its $UBVR$ and JK light curves using two gas-dynamical models with different regions of shock interaction: one with a hot line along the stream from the Lagrange point L_1 and one with a hot spot on the accretion disk. The hot-line model can better describe the quiescent state of the system: the maximum χ^2 for the optical light curves does not exceed 207, whereas the minimum residual for the hot-spot model is $\chi^2 > 290$. The shape of the eclipse is almost identical in both models; the main differences are in interpreting out-of-eclipse portions of the light curves, whose shape can vary in the transition from one orbital cycle to another. The hot-spot model is not able to describe variations of the system's brightness at orbital phases $\varphi \sim 0.1$–0.6. The rather complex behavior of the observed flux in this phase interval can be explained in the hot-line model as being due to variations of the temperature and size of the system. Based on the analysis of a sequence of 20 B curves of OY Car, we conclude that the flux variations in the primary minimum are due to variations of the luminosity of the accretion disk, whereas the flux variability in the vicinity of the orbital peak is due to the combined effect of the radiation of the disk and hot line. The JK light curves of OY Car in the quiescent state and during a small flare also indicate preference for the hot-line model, since the primary minimum and the flux near quadratures calculated using the hot-spot model are not consistent with the observations. © *2003 MAIK "Nauka/Interperiodica".*

1. INTRODUCTION

Cataclysmic close binary systems are among the most interesting non-steady-state astrophysical objects, due to the intense mass transfer between the components. Their short orbital periods enable the determination of the characteristics and parameters of the system over comparatively short observational times.

The light curves and radial-velocity curves of these systems indicate that they consist of a white dwarf and cool main-sequence star. The latter fills its Roche lobe, resulting in an outflow of matter through the vicinity of the inner Lagrange point L_1. Further, this matter is captured by the white dwarf's gravitation and forms an accretion disk, halo, and intercomponent envelope. The existence of the accretion disk is confirmed by the profile of the eclipse of the white dwarf and the surrounding material by the cool component of the system. However, light curves of eclipsing close binaries display some additional features that cannot be described in simple "cool star–white dwarf–accretion disk" models. In particular, the vast majority of light curves of eclipsing close binaries display a so-called "orbital peak." Gorbatskiĭ [1] and Smak [2] suggested that this is due to a hot spot at the edge of the accretion disk, where the stream from L_1 collides with the disk. Over the last 30 years, the hot-spot model has been widely used to interpret the light curves of cataclysmic binaries (see, for example, [3]).

Gas-dynamical studies of the mass transfer in close binaries [4–9] showed that the stream and accretion disk are morphologically a single formation and that their interaction is shockless. Naturally, in this case, the temperature at the point of contact between the stream and disk does not increase, so that the hypothesis that there is a hot spot on the accretion disk must be abandoned. Three-dimensional gas-dynamical calculations of mass transfer in an interacting close binary [4–9] have indicated that, in the steady-state case, a shock interaction resulting

1063-7729/03/4703-0214$24.00

Table 1. Parameters of the OY Car components

The system, $P = 0^d.063121$ [17]			Hot dwarf			Cool star		
i, deg	$q = M_1/M_2$	a_0, 10^{10}, cm	R_1/a_0	T_1, K	M_1, $M_\odot$	R_2/a_0	T_2, K	M_2, $M_\odot$
79(2) [14]	4–7 [14]	4.8(3) [14]	0.013(4) [14]	25 000 [16]	0.95 [14]	0.23(6) [14]	3000 [14]	0.14 [14]
81 [28]	9.8(3) [29]	4.3(2) [29]	0.0182(3) [29]	$\geq$ 20 000 [31]	0.33 [22]	0.209 [29]		0.07 [29]
83.3 [29]				$\leq$15 000 [28]	1.26 [18]			
				15 000 [23]	0.68 [29]			
					0.69 [17]			
82	9.8		0.0182	15 000			3000	

Note: The bottom row presents parameters derived from our analysis of the OY Car light curves. The error in the last digit of a parameter is given in parentheses.

in a temperature increase occurs when the matter flowing around the accretor but not yet captured by the disk collides with the stream from L_1. This interaction forms an extended shock wave oriented along the stream [4–6, 10] (the "hot line"), whose radiation makes it possible to understand certain observed effects in the light curves of cataclysmic variables [11, 12], in particular, the occurrence of regular and irregular peaks during eclipses of the accretion disk by the donor star. Comparisons between models with a hot spot and a hot line [11, 12] have presented conclusive evidence in favor of the latter type of model for the interpretation of close-binary light curves.

Eclipsing close binaries, whose light curves can be used to investigate the flow structure, are rare and do not form a homogeneous group. Therefore, it is of interest to consider close binaries with various features in their light curves and to analyze the suitability of various gas-dynamical models for their interpretation. Here, we present our analysis of light curves of the SU UMa cataclysmic variable OY Car.

2. GENERAL INFORMATION ABOUT OY Car

The variability of OY Car (= *S*6302) was discovered by Hoffmeister [13] in 1959; however, this star was observed little in the subsequent two decades. In the beginning of the 1980s, interest in this system increased substantially, leading to intense observations. Comprehensive summaries of the photometric observations are given by Vogt *et al.* [14], Vogt [15], Schoembs *et al.* [16, 17], and Cook [18], of IR photometric observations by Berriman [19, 20] and Sherrington *et al.* [21], and of spectral observations by Bailey and Ward [22], Hessman *et al.* [23], and Harlaftis and Marsh [24].

The light curve of the system in the inactive state is typical of eclipsing close binaries. A pronounced peak with its maximum at phase $\sim$0.75 is observed in each orbital cycle prior to the eclipse of the primary. The times of the onset and end of the ingress into eclipse for the white dwarf, disk, and hot region of the shock are clearly visible in the eclipse curve.

In the active state, the system displays a number of peculiarities. The flare activity of OY Car classifies it as an SU UMa variable; these are dwarf novae with orbital periods shorter than 3 h. Flares of this type of star are divided into two separate classes: regular flares, which are brief and irregularly distributed in time, and superflares. The latter are more prolonged, brighter, and less frequent; however, at the same time, they are more predictable. In the case of OY Car, the regular flares occur every 25–50 days and have amplitudes up to $\simeq 3^m$ and durations of about 3 days. Superflares occur approximately once a year. Their amplitude reaches 4^m, and they may last for up to 2 weeks. Photometric observations of the system in these periods have been carried out by Krzeminski and Vogt [25], Schoembs [26], and Bruch *et al.* [27].

Observations of OY Car are analyzed in [18, 22, 23, 28, 29]. The orbital parameters and mass ratio of the components were derived from radial-velocity measurements. The size of the disk and the white dwarf, as well as the orbital inclination, were estimated based on the shape of the primary minimum. The spectrum and comparisons of the photometric parameters of the system in various colors have been used to determine the effective temperature of the cool component and, with lower accuracy, the temperature of the hot star. The mass of the white dwarf was estimated based on its radius using the Hamada–Salpeter relation [30]; later, the mass of the cool component was also derived. The period of the system was determined with good accuracy from an extensive set of photometric observations. Table 1 presents some parameters of OY Car.

Below, we analyze $UBVR$ [17, 27, 29] and JK [21] light curves of OY Car and derive the characteristics of the main gaseous components of the system: the accretion disk and the shock region responsible for the formation of the orbital peak.

3. BASIC ASSUMPTIONS OF THE MODEL

The observed radiation of a binary system is generally a combination of the contributions of both of its components, the accretion disk, and gaseous structures forming in the system due to the outflow from the donor star. According to gas-dynamical calculations, the shape of the intercomponent gaseous envelope in the system is rather complex, and a detailed analysis of its radiation represents a very sopisticated problem. As a first approximation, given the low gas density in the intercomponent envelope, we will ignore its contribution to the total radiation. We also assume that the contribution to the visible radiation from the stream from L_1 is negligible due to the low temperature of the gas in the stream. In our present model, we take into account only the radiation from the system's components, the accretion disk, and the shock-interaction region.

In general, light-curve analyses can be used to determine the parameters of these systems. However, since each source has some temperature and size, and since the temperature can vary across the surface of the star, even a restricted model will be specified by a set of more than 20 parameters. Naturally, the large number of parameters involved complicates their reliable determination. Therefore, we selected a set of parameters whose values are known with high certainty and fixed them in the model. For example, we adopted the values in Table 1 for the stellar components.

Imposing additional constraints enabled us to restrict the number of free parameters and thereby simplify the model. Here, we aim to obtain the characteristics only of the accretion disk and the region of shock interaction by analyzing the light curves. We derive solutions using two gas-dynamical models with different locations for the region of shock interaction: (a) in a hot line along the stream from L_1 (this model is described in [32]) and (b) in a hot spot on the accretion disk (the light curve for this model is synthesized in [33]). Comparisons between the results will help distinguish between these gas-dynamical models.

4. OPTICAL LIGHT CURVES OF OY Car IN ITS INACTIVE STATE

Schoembs *et al.* [17] carried out photometry of OY Car in its inactive state using a multichannel photometer with a time resolution 2 s. They present continuous sets of B observations during six nights from January 26 to February 2, 1984 (HJD 2445725–2445733). The shape of the light curves varies substantially. Those with flat portions between the orbital peaks alternate with those displaying flares between the peaks. No periodicity in the occurrence of the flares has been detected.

Twenty light curves at orbital phases from −0.5 to +1.5 were selected from the six sets of observations obtained on different nights, labeled with numbers N from 1 to 20. When constructing the Nth curve, observations for partial orbital light curves (i.e., those observed at the beginning and end of the observations) were assigned to the nearest total light curve. When an observational set was divided into separate orbital curves, the interval of orbital phases was selected so that the fluxes at the beginning and end of the light curve were roughly the same. As a rule, this break fell at phases $\varphi \sim 0.3$–0.4, However, if a secondary peak (flare) was observed in this phase interval at the beginning or end of the curve, the break was shifted to a less perturbed portion of the curve.

The out-of-eclipse portions of individual observed light curves were averaged. The averaged portions of the curves are represented by $n = 23$–33 regular dots with the rms error $\sigma_j \sim 0^m.010$–$0^m.015$. Observations at the minimum of the light curve were not averaged. Generally, four to eight points were obtained during an eclipse of the white dwarf. Unaveraged observations were assigned the error $\sigma \simeq 0^m.03$, which roughly corresponds to the error of a single observation [17]. From the collection of 20 observed light curves, we selected the $N = 14$ curve, which had the minimum flux ($\delta B = 3^m.83$ relative to the comparison star) at the first quadrature ($\varphi = 0.25$), and used this magnitude $\delta B = 3^m.83$ as the zero level for all remaining light curves. All 20 individual light curves were expressed in magnitude differences ΔB relative to the magnitude of the system at the first quadrature of the $N = 14$ light curve:

$$\Delta B = B_N^{obs}(\varphi) - B_{14}^{obs}(\varphi)$$
$$= -2.5\log(F_N^{obs}(\varphi)/F_{14}^{obs}(0.25)).$$

This means that we use the same energy unit—the observed flux from the system at orbital phase $\varphi = 0.25$ for the $N = 14$ light curve—for the entire set of 20 light curves. This enables us to estimate the brightness differences between curves at each phase, and thereby to use variations of the flux levels, as well as of the shape of the light curve, when comparing the observed and synthesized curves. In other words, this is one way to impose additional restrictions on the range of allowed parameters of the system.

The shapes of successive light curves of OY Car in its inactive state indicate that some non-steady-state processes occur in the system even during this

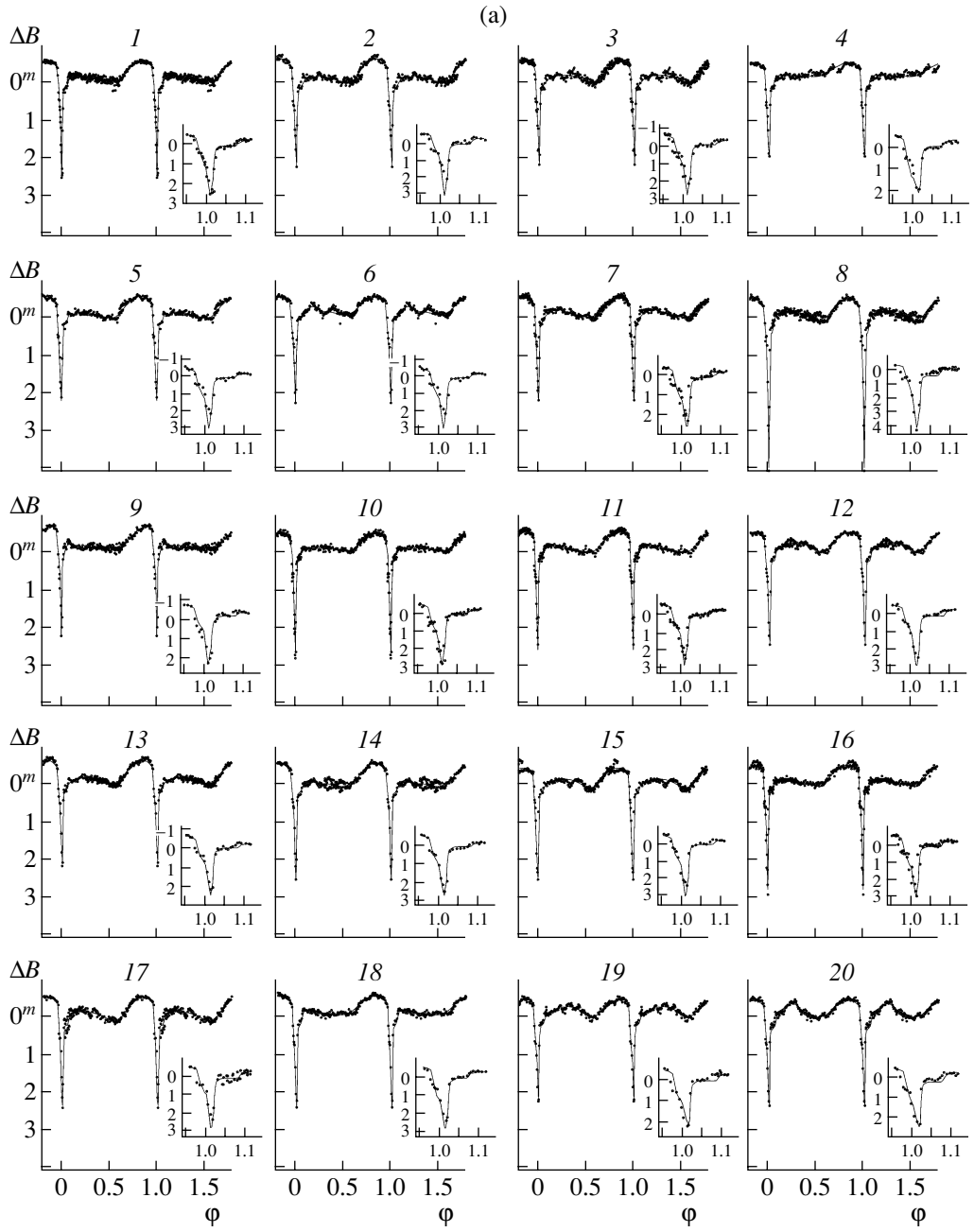

Fig. 1. (a) Individual B light curves of OY Car in magnitude differences relative to the flux observed at quadrature ($\varphi = 0.25$) for the $N = 14$ light curve. The solid curves indicate theoretical light curves synthesized in the hot-line model. The inset in each plot presents the eclipse portion of the corresponding light curve. (b) Contributions of the white dwarf (*1*), donor star (*2*), elliptical disk (*3*), and hot line (*4*) to the total flux in arbitrary units (see text) for the corresponding light curve of OY Car.

brief period of time (Fig. 1a). There are variations in both the depth of the primary minimum (with amplitudes up to $\simeq 1^m$–2^m) and in the amplitude of the orbital peak (up to $\simeq 0^m.5$) associated with the region of shock radiation. The shape of the curve varies at orbital phases $\varphi \sim 0.2$–0.6 from cycle to cycle, precisely in the phase interval when the radiation from the hot spot cannot reach the observer.

We analyzed 20 individual light curves using the hot-line model in order to identify the model components whose variations result in the observed variations of the shape of the orbital curves. In addition, it was important to confirm that the hot-line model provides a better fit than the hot-spot model, not only in the analysis of the light curve averaged over numerous cycles, but also for each of the 20 individual light curves, despite the substantial cycle-to-cycle variations.

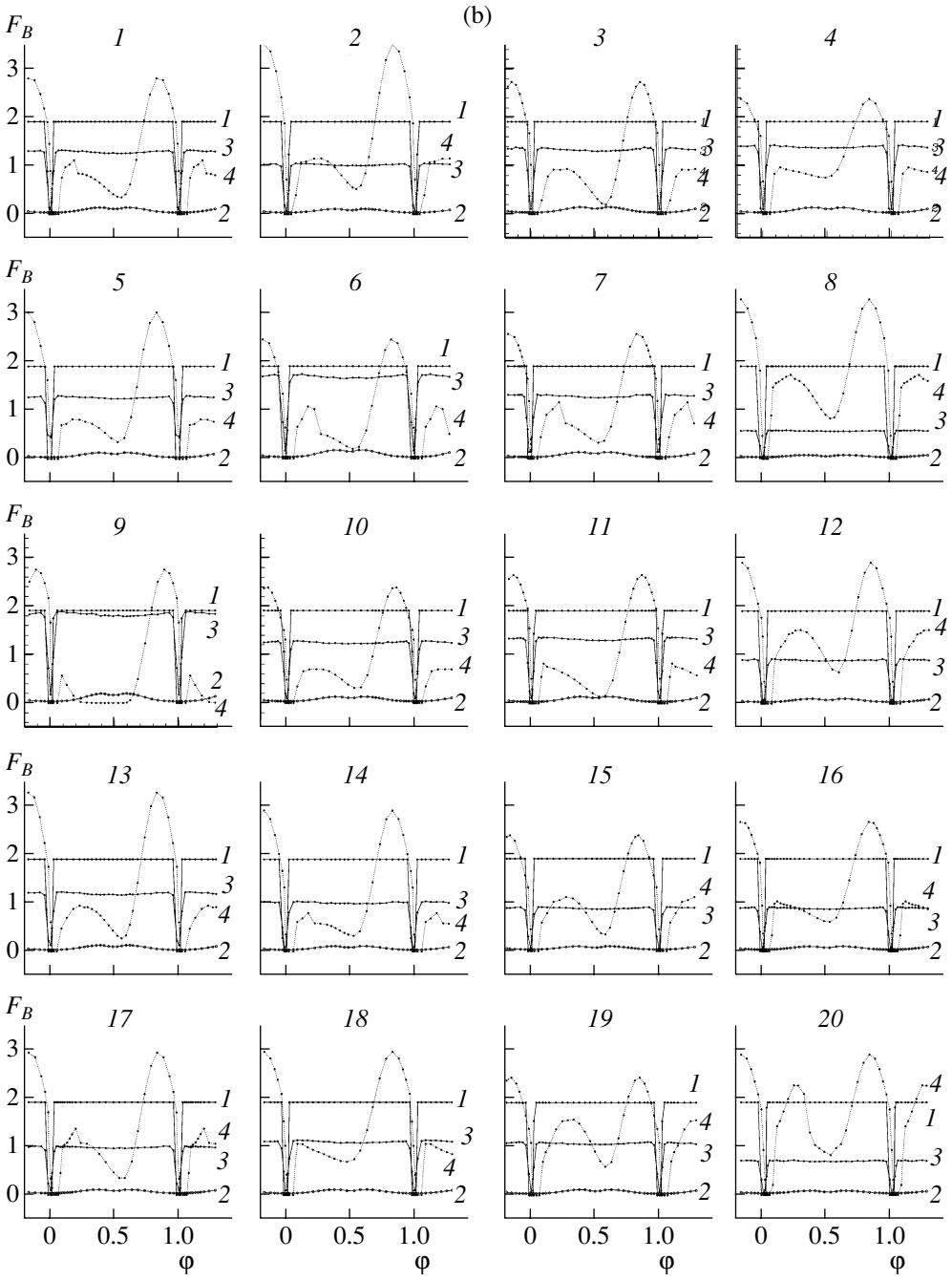

Fig. 1. (Contd.)

To construct the theoretical light curve, we calculated the flux from the system's components $F(X, \varphi)$ for a specified set of parameters X and for a sequence of orbital phases φ. The resulting $F(X, \varphi)$ values were given in arbitrary units. They can be transformed into generally accepted units (per unit wavelength interval) using the expression $f = Fa_0^2 \times 10^{-12}$ erg/s cm^3, where a_0 is the distance between the centers of mass of the stars in centimeters. As noted above, the N analyzed light curves ($N = 1$–20) are given in magnitude differences ΔB, where $\Delta B = 0^m.0$ corresponds to the average observed flux at the first quadrature for the $N = 14$ light curve. Accordingly, when translating the theoretical fluxes $F_N^{th}(X, \varphi)$ to magnitudes $\Delta B_N^{th}(X, \varphi)$ when constructing the synthesized light curves, we used the first-quadrature flux $F_{14}^{th}(0.25)$ for the theoretical curve that gives the best fit to the observed $N = 14$ light curve; i.e., the theoretical magnitude of the

system at phase φ for light curve N will be

$$\Delta B_N^{th}(\varphi) = -2.5\log(F_N^{th}(\varphi)/F_{14}^{th}(0.25)).$$

This imposes an additional restriction on the range of allowed parameters. If we interpret a single light curve rather than a sequence of homogeneous curves, the first-quadrature flux corresponding to the given trial curve is used to translate the calculated flux to magnitudes to construct the trial theoretical curve (in magnitudes). In this case, there is no need to first subtract the first-quadrature flux in magnitudes from the observed light curve. To compare the synthesized and observed curves, it is sufficient to shift the calculated trial light curve so that the observed and calculated fluxes (in magnitudes) at the first quadrature coincide. We selected the best-fit theoretical light curve based on a minimum residual χ^2 derived from comparison with the observed curve.

We carried out the calculations for the sequence of 20 B light curves in two stages. We first fixed five of the 18 unknown parameters, which had been determined with sufficient certainty in other studies. The values adopted for these parameters are presented in the bottom row of Table 1. We thus reduced the number of unknown parameters to 13 at the first stage of our calculations. The allowed values of most of these were additionally restricted.

For example, in accordance with [15–17], the maximum radius of the disk was restricted to the interval $a_{\max}/\xi = 0.53$–0.62, since analyses of the shapes of eclipses yield the average radius $a_d/\xi = 0.58$ for $q = 9.8$ (ξ is the distance between the center of mass of the white dwarf and the inner Lagrange point, $\xi/a_0 = 0.7159$). As a rule, when the structure of eclipses is analyzed, only the time of the beginning of the disk eclipse is determined with certainty, whereas the time of the egress from the eclipse is determined fairly uncertainly [34]. On the other hand, three-dimensional hydrodynamical calculations of flows in cataclysmic variables [35] indicate that, in the inactive state of the system, the accretion disk is elliptical and the longitude of its periastron lies in the interval $\alpha_e \sim 150°$–$170°$. Given this orientation of the disk, the radius derived from the moment of the ingress of the eclipse is close to the radius at apoastron of the disk. Therefore, it was the radius of the disk at apoastron rather than its average value that we restricted in our calculations.

The other desired parameters describe the shape of the disk and the shape and size of the hot line:

(1) the eccentricity of the disk (we assumed its value in the inactive state does not exceed $e \sim 0.22$);

(2) the paraboloid constant A_p specifying the thickness of the outer edge of the disk z/a, along with the radius of the disk at periastron (for a thin disk, $A_p \sim 5$–7);

(3) the azimuth of the disk periastron α_e, measured in the direction of the orbital motion of the secondary, from the straight line connecting the centers of mass of the components;

(4) the brightness temperature T_b in the boundary layer where the disk material is accreted onto the compact star ($T_b \geq T_1$);

(5) the parameter α_g specifying the variation of the brightness temperature with the disk radius in accordance with the formula $T_r = T_b(R_1/r)^{\alpha_g}$ (we assumed $\alpha_g \sim 0.6$–0.75);

(6) the shape of the hot line—a truncated ellipsoid with semiaxes a_v, b_v, c_v extended toward the inner Lagrange point L_1 (the lateral surface of this ellipsoid coincides with the tangent to the elliptical disk for any disk orientation, while its center is located in the orbital plane inside the disk at some distance from its edge; the procedure used to construct the shape of the hot line is described in detail in [32]);

(7) the maximum brightness temperature of the hot line on its windward ($T_{\max}^{(1)}$) and leeward ($T_{\max}^{(2)}$) sides;

(8) the y coordinate on the axis of the hot line $y_{\min}$, where the heating of the gaseous stream by the shock wave becomes zero (i.e., the temperature is equal to the temperature the matter would have in the absence of the shock);

(9) the shift Δy along the axis of the hot line between the points with the maximum values $T_{\max}^{(1)}$ and $T_{\max}^{(2)}$ from the windward and leeward sides (generally, $\Delta y/a_0 < 0.05$).

The calculations indicate that the values for the eccentricity of the disk, A_p, and α_g derived from the analysis of the 20 light curves are fairly closely clustered around their average values. At the second stage of the calculations, we also fixed the values of these parameters to be $e = 0.185$, $A_p = 5.400$ (which corresponds to an flaring angle for the outer edge of the disk $\beta_d = 3.^\circ 9$), and $\alpha_g = 0.70$. A trial run was made for Δy in the interval 0.0–0.60. As a result, the number of free parameters was decreased to nine.

Table 2 presents the resulting parameters of the disk and hot line, as well as the values of other quantities that depend on them. Asterisks denote light curves whose shapes are distorted by short flares at orbital phases $\varphi \sim 0.5$. Table 2 also presents the observed flux of OY Car relative to the comparison star averaged for phase intervals $\varphi = 0.99$–1.01, 0.10–0.16, 0.50–0.60, and 0.80–0.86.

Since only one of the solutions (for the $N = 14$ curve) had a lower than critical significance level $\chi^2_{0.001,n}$ ($\chi^2_{0.001,n} = 49.7$–64.0 for $\alpha = 0.001$, with the number of degrees of freedom being $n = 23$–33 for

Table 2. Theoretical parameters of OY Car in its inactive state (from B observations), derived from the light curves of [17] and the hot-line model

Parameter	Light curve number									
	1st set of observations			2nd set of observations				3rd set of observations		
	1	2	3*	4	5	6*	7	8	9*	10
n	33	27	30	23	24	25	29	32	29	30
a/a_0	0.364	0.345	0.374	0.345	0.346	0.355	0.363	0.324	0.358	0.356
$a_{\max}/\xi$	0.603	0.571	0.619	0.572	0.572	0.588	0.601	0.536	0.592	0.589
α_e, deg	168.8	159.0	171.7	182.3	161.8	166.0	170.6	148.1	154.9	165.7
T_b, K	22 461	21 069	22 821	22 592	22 134	23 820	22 493	18 270	24 279	22 191
a_v/a_0	0.065	0.057	0.055	0.097	0.062	0.063	0.068	0.075	0.06 7	0.056
b_v/a_0	0.352	0.361	0.334	0.556	0.404	0.384	0.378	0.423	0.20 3	0.352
c_v/a_0	0.021	0.019	0.023	0.018	0.021	0.023	0.022	0.020	0.02 7	0.019
$y_{\min}/a_0$	0.265	0.238	0.248	0.274	0.247	0.302	0.266	0.267	0.203	0.251
$T^{(1)}_{\max}$, K	14 747	18 031	14 782	16 565	15 838	10 592	13 958	19 562	13 691	13 853
$T^{(2)}_{\max}$, K	11 181	13 947	12 246	10 258	13 187	9318	10 612	12 587	12 934	11 611
$\langle T^{(1)}\rangle$, K	6367	6184	6364	3653	5068	5777	5707	5854	8047	5739
$\langle T^{(2)}\rangle$, K	5773	5166	4775	4153	4499	5713	5383	4825	6888	4954
$F^{\rm obs}_{0.99-1.01}$	3.0(2)	3.8(2)	3.9(2)	4.8(2)	4.3(2)	3.8(2)	3.9(2)	0.7(2)	3.8(2)	2.3(2)
$F^{\rm obs}_{0.10-0.16}$	34.6(4)	33.1(5)	33.6(3)	33.7(5)	33.4(7)	37.0(6)	35.1(5)	34. 0(3)	33.6(3)	31.1(3)
$F^{\rm obs}_{0.50-0.60}$	30.2(5)	30.3(4)	29.6(5)	37.0(4)	29.8(3)	32.6(3)	30.0(4)	27. 7(2)	31.5(3)	30.0(3)
$F^{\rm obs}_{0.80-0.86}$	49.4(3)	53.9(7)	49.5(3)	46.9(3)	49.7(5)	50.1(5)	50.1(5)	48. 7(4)	52.9(6)	45.5(5)
$\chi^2_{0.001,n}$	64.0	55.5	59.7	49.7	51.2	52.6	58.3	62.6	58.3	59.7
χ^2	74.8	167	107	179	123	173	173	271	72.2	121
	4th set of observations			5th set of observations			6th set of observations			
	11	12*	13	14	15*	16	17	18	19*	20*
n	30	27	29	27	28	34	30	28	29	31
a/a_0	0.361	0.358	0.367	0.358	0.358	0.356	0.366	0.345	0.360	0.351
$a_{\max}/\xi$	0.598	0.593	0.607	0.593	0.592	0.589	0.605	0.571	0.595	0.581
α_e, deg	160.1	172.6	169.3	167.7	169.2	168.2	170.3	160.3	184.0	175.2
T_b, K	22 599	20 652	22 163	21 210	20 595	20 591	21 186	21 459	21 497	19 500
a_v/a_0	0.078	0.051	0.046	0.056	0.045	0.081	0.063	0.104	0.04 1	0.069
b_v/a_0	0.313	0.415	0.348	0.397	0.368	0.413	0.355	0.464	0.46 7	0.555
c_v/a_0	0.025	0.019	0.020	0.018	0.019	0.019	0.023	0.020	0.01 7	0.018
$y_{\min}/a_0$	0.245	0.264	0.256	0.278	0.231	0.247	0.243	0.274	0.255	0.328
$T^{(1)}_{\max}$, K	15 690	17 485	12 968	12 164	15 990	18 996	18 597	17 334	16 215	15 304
$T^{(2)}_{\max}$, K	12 987	10 878	11 483	10 846	11 990	12 177	12 383	11 582	10 023	9270
$\langle T^{(1)}\rangle$, K	6548	5981	6070	5177	5516	4802	6012	4236	5124	5321
$\langle T^{(2)}\rangle$, K	5096	4982	5897	5565	4332	4625	4871	4713	4701	4873
$F^{\rm obs}_{0.99-1.01}$	3.3(2)	3.0(2)	4.0(2)	2.8(2)	2.8(2)	2.0(2)	3.2(2)	3.2(2)	3.8(2)	3.4(2)
$F^{\rm obs}_{0.10-0.16}$	34.2(3)	33.3(4)	32.2(2)	29.7(4)	30.7(3)	31.6(3)	33.3(4)	34. 0(4)	32.8(3)	32.9(4)
$F^{\rm obs}_{0.50-0.60}$	29.7(4)	29.2(3)	28.9(2)	28.5(4)	26.1(2)	28.9(3)	27.4(3)	32. 2(3)	29.9(4)	30.2(4)
$F^{\rm obs}_{0.80-0.86}$	49.2(3)	46.5(3)	52.9(7)	48.3(3)	44.0(0)	46.2(6)	48.1(3)	49. 9(5)	45.4(6)	45.9(4)
$\chi^2_{0.001,n}$	59.7	55.5	58.3	55.5	56.9	65.5	59.7	56.9	58.3	61.2
χ^2	61.2	106	97.9	46.8	167	258	63.8	172	185	176

Note: n is the number of regular points in the averaged curve. The parameters of the disk and hot line are derived for fixed $q = M_1/M_2 = 9.8$, $i = 82°$, $T_2 = 3000$ K, $T_1 = 15\,000$ K, $R_1 = 0.0182a_0$, $\alpha_g = 0.7$, $e = 0.185$, and $A_p = 5.4$ (this corresponds to a flaring angle for the outer edge of the disk $\beta_d = 3°.9$). The parameter $\Delta y \sim 0.001$–0.02 for most of the light curves. The maximum and minimum radii of the disk for the known e are determined using the formulas $a_{\max} = a(1+e)$ and $a_{\min} = a(1-e)$, where a is the semimajor axis of the disk. The average radius of the red dwarf is $\langle R_2\rangle/a_0 = 0.2144$. The asterisks mark orbital cycles with flares.

various curves; see Table 2), the effect of varying a particular parameter can be estimated by imposing some other limit for the residual in place of the critical limit; for example, the obtained minimum residual can be increased by 10%. For most parameters, the interval of possible variations does not exceed 1–2% of their optimum value. Only for the maximum brightness temperature of the hot line were deviations from the optimum value as large as 8–10% and 2–3% for its windward and leeward sides, respectively; $\Delta y \sim 10$–12%, $a_v \sim 5$–7%, and $\alpha_e \sim 9$–12%.

The solid curves in Fig. 1a represent theoretical light curves synthesized with the parameters from Table 2, reduced to the flux $F_{14}^{th}(0.25)$. The points show the individual (nonaveraged) light curves in magnitude differences relative to the observed first-quadrature flux of the $N = 14$ curve. The curves are numbered in accordance with the notation in Table 2. The inset shows the eclipse portion of the corresponding light curve. The analysis of the contributions from the white and red dwarfs, the elliptical disk, and the hot line indicates (see Fig. 1a) that the contribution of the red dwarf is insignificant at optical wavelengths given the high component mass ratio of OY Car (it does not exceed 1.5–2%).

The out-of-eclipse contribution from the white dwarf is constant for all the curves, at 30–37% of the total maximum flux (at phases $\varphi \sim 0.85$). The out-of-eclipse flux from the elliptical disk is also essentially constant due to the small eccentricity; overall, it is lower than the flux from the white dwarf, and displays a comparable magnitude only in certain individual cycles ($N = 9$, $N = 6$). Since the radius of the disk varies insignificantly, the variations of the disk luminosity are due to fluctuations of T_b. Due to the law for the radial variation of the temperature adopted in our model, the inner parts of the disk that are $\sim 0.25R_d$ from the white dwarf yield roughly the same flux as the remaining outer three quarters, since the temperature of the outer parts of the disk is comparable to that of the red dwarf ($T_d \sim 2000$–3000 K).

The orientation of the disk proved to be close to that obtained from hydrodynamical calculations [35], $\alpha_e \sim 150°$–$185°$; the longitude of the disk periastron fluctuates only slightly about its average value, $\sim 165°$. This orientation of the elliptical disk makes it possible to describe the shapes of both the eclipse and out-of-eclipse portions of the light curves with good accuracy (Fig. 1a). For smaller longitudes of the disk periastron, the theoretical curve remains fairly consistent with the observations. However, the shape of the curve at $\varphi \sim 0.3$–0.8 is fit more poorly. It is not possible to fit the shape of the eclipse well when $\alpha_e > 190°$: its depth decreases and its shape changes, since the eclipse of the hot line shifts toward later orbital phases relative to the eclipses of the white dwarf and disk, which are symmetrical about $\varphi = 0.0$. Since the model assumes that the leeward side of the gaseous stream is tangent to the edge of the disk, the orientation of the disk indirectly affects the visibility conditions for the bright part of the hot line from both its windward and leeward sides.

Figure 2 combines all 20 average light curves obtained by Schoembs *et al.* [17]. It is apparent that the shape of the curves is essentially reproduced from cycle to cycle and that the curves fluctuate about the average position. The variations are largest near the primary and secondary minima, and are somewhat smaller near the orbital peak. Note that the secondary minimum in this system is basically due to the effects of the eclipse of the hottest part of the shock wave by the edge of the disk from its windward side, rather than to eclipses of the red dwarf, whose luminosity is very low.

The procedure of matching all the synthesized light curves to the same flux $F_{14}^{th}(0.25)$ enables us to determine the component whose variations mainly affect the amplitude of the orbital peak and the depth of the primary minimum of the light curves.

To obtain quantitative estimates, we selected four reference points in the light curves, at phases $\varphi \sim 0.0$ (primary minimum), 0.13 (egress from the eclipse and the region around the secondary maximum of the flux from the hot line), 0.55 (close to the secondary minimum of the flux from the hot line, specified by the eclipse of the line by the disk edge), and 0.83 (the maximum of the peak, the region adjacent to the primary maximum of the hot-line flux). Figure 2 presents the positions of various components at these phases. The real times of the maxima and minimum of the curves may differ by $\Delta\varphi \sim \pm 0.06$–$0.08$ to one or the other side of the selected average positions. Such deviations often indicate the presence of flares in the light curves.

The asymmetrical shape of the eclipse (the steep ingress into eclipse and smoother egress from eclipse) is consistent with the fact that the projections of the hottest regions of the disk and hot line onto the plane of the sky are displaced from the line connecting the centers of the stars. In the case of a circular disk, the center of its eclipse (either total or partial) would be at phase $\varphi = 0.0$, as would the center of the white-dwarf eclipse. The elliptical shape of the disk shifts the phase of the deepest eclipse by $\Delta\varphi \sim 0.005$ from phase $\varphi = 0.0$. The center of the hot-line eclipse is shifted by an even larger amount ($\Delta\varphi \sim 0.04$ from phase $\varphi = 0.0$).

In cycle $N = 8$, a substantial decrease of the system flux in the primary minimum is observed compared to the adjacent cycles. The analysis of the contributions from the components (Fig. 1b) indicates

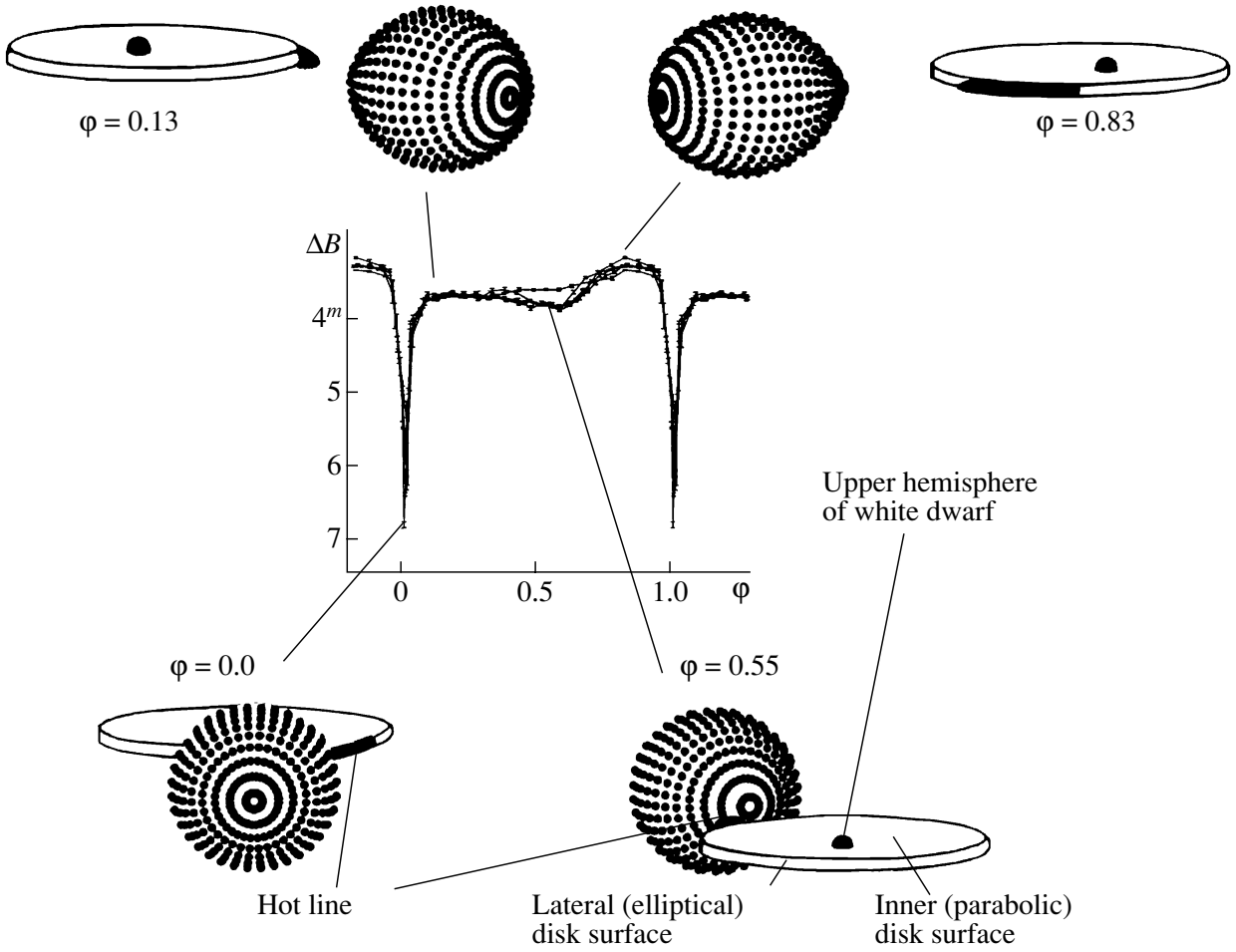

Fig. 2. The red dwarf, disk (the contours of the disk edge are shown schematically), and the hot line (its surface is shaded for better contrast) at various phases of the orbital cycle (at reference points; see the text). The sum of all 20 average light curves obtained by Schoembs *et al.* [17] is presented in the center.

that the luminosity of the disk in cycle $N = 8$ decreased by factors of 2.3 and 3.2 compared to its luminosity in the adjacent cycles $N = 7$ and 9, respectively. We can see from Fig. 2 that the disk eclipse is partial. However, the main flux comes from the inner regions of the disk, which are heated to temperatures > 5000 K, while the outer parts of the disk, whose temperature is comparable to that of the red dwarf ($T_d \sim 2000$–3000 K), do not contribute appreciably to the total flux. The temperature decrease along the radius of the disk is rather steep—the hottest regions of the disk with temperatures > 5000 K are no further than $(0.20$–$25)R_d$ from the white dwarf. Therefore, the maximum temperatures of the inner parts of the disk in cycles $N = 7$ and 9 are $\sim 22\,500$–$24\,300$ K, while the maximum temperature in cycle $N = 8$ is $\sim 18\,300$ K (Table 2). When the temperature of the inner parts of the disk decreases, so does the size of the central part of the disk giving rise to the bulk of the flux (the average radius of the radiating region in cycle $N = 8$ is $\sim 0.16a_0$, while it is $0.21a_0$ and $0.23a_0$ in cycles 7 and 9, respectively). Consequently, the residual flux from the disk during its eclipse by the red dwarf also decreases. This is precisely the reason for the substantial increase of the depth of the eclipse in the primary minimum in the $N = 8$ light curve.

Figures 3a–3f display the dependences between the observed maximum ($\varphi \sim 0.83$) and minimum ($\varphi \sim 0.0$) fluxes from the study of Schoembs *et al.* [17] and the calculated fluxes from the disk (Figs. 3a, 3d), the hot line (Figs. 3b, 3e) and their sum (Figs. 3c, 3f) at the corresponding phases. The theoretical fluxes F are given in arbitrary units. The squares mark light curves whose shapes are distorted by small flares.

These figures show that the height of the orbital peak depends on the combined contribution of the radiation from the disk and the hot line (Fig. 3c). The scatter of the dependences between the fluxes observed at the light-curve maxima and the calculated fluxes from the disk or hot line (Figs. 3a, 3b) is rather

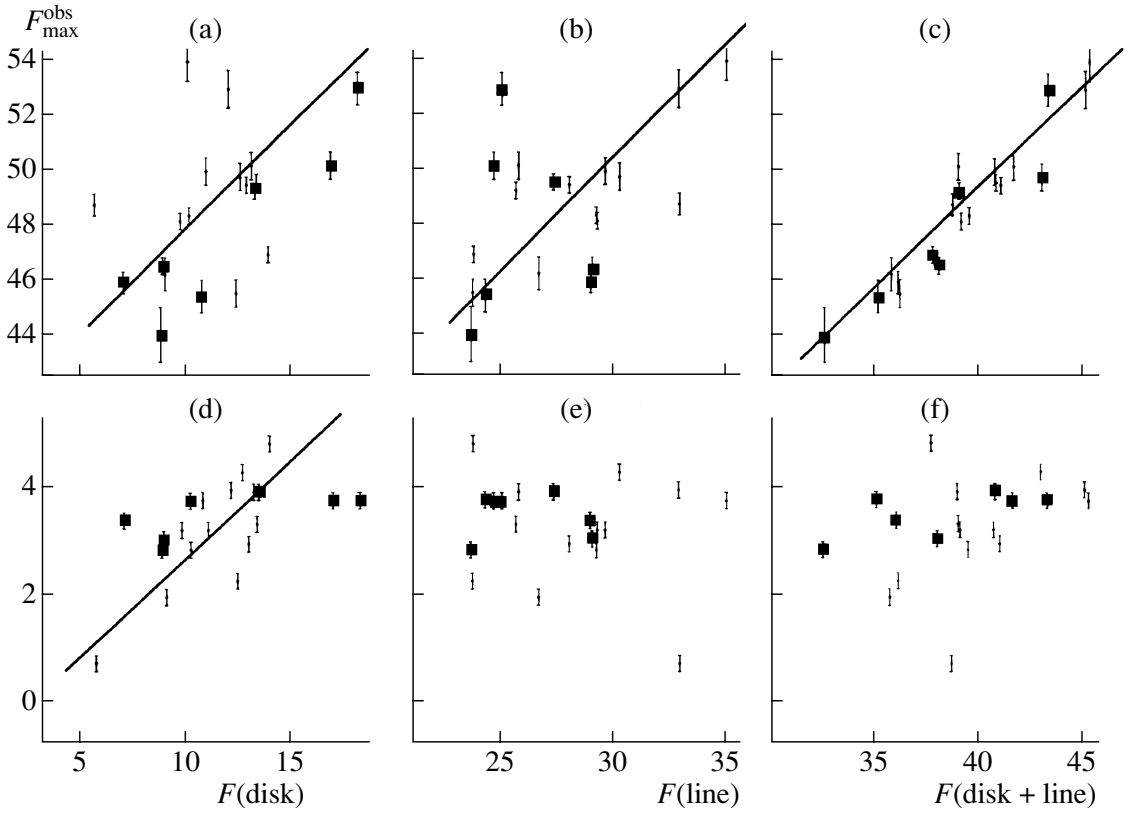

Fig. 3. (a–c) Relationships between the observed flux (in arbitrary units) at phases 0.80–0.86 (the orbital peak) and the theoretical fluxes (in arbitrary units) at phase $\varphi = 0.83$ from (a) the disk, (b) the hot line, and (c) the sum of these two components, calculated with the parameters from Table 2; (d–f) the same dependences for the fluxes observed in the primary minimum ($\varphi \sim 0.99$–1.01) and calculated for phase $\varphi = 0.0$.

large; nevertheless, some correlation can be seen. The flux in the primary minimum is specified only by the flux from the disk (Fig. 3d). There is no relationship between the observed flux in the primary minimum and the flux from the hot line (Figs. 3e, 3f). This is apparently due to the fact that the fairly extended accretion disk is partially eclipsed in the minimum (Fig. 2), whereas the eclipse is almost total for the relatively small hot portion of the shock.

Attempts to fit the orbital light curves of Schoembs *et al.* [17] with models with a hot spot on the side of a circular disk [33] were not successful. For each curve $N = 1$–20, the minimum residual is $\chi^2 \geq 700$. The shapes of the light curves in this model are similar to those in Fig. 4. It is evident that the hot-spot model can adequately reproduce the shape of the eclipse; however, it is unable to fit the out-of-eclipse parts of the orbital light curves with sufficient accuracy. The orbital light curves $N = 1$–20 from [17] are described considerably better using the hot-line model: the residual χ^2 does not exceed $\chi^2 \sim 270$ for light curves $N = 1$–20; it is lower than the critical χ^2 level for the $N = 14$ curve, and is comparable to the corresponding $\chi^2_{0.001,n}$ for the $N = 1$, $N = 11$, and $N = 17$ curves.

Table 3 presents the parameters of the disk and hot-line models derived from the U, B, R ($\lambda_{\text{eff}} = 6517$ Å), and white light ($\lambda_{\text{eff}} = 4960$ Å, W) OY Car light curves of Wood *et al.* [29], which were averaged over several dozen orbital cycles. When the calculated parameters for the B curve (Tables 2 and 3) and the shape of the average B light curve [29] are compared to the individual orbital curves [17], it is obvious that the average light curve is close to the least perturbed individual orbital curves in this filter, for example, to the $N = 13$ curve. The upper part of Table 3 presents the results for the average light curves of OY Car using the hot-line model; the lower part presents the parameters obtained for the hot-spot model [33]. The errors of the last decimal places of the corresponding parameters calculated for an arbitrary residual level exceeding the minimum residual by 10% are given in parentheses. The minimum residual in the hot-spot model is more than a factor of 1.5 higher than in the hot-line model.

Figure 4a presents the averaged U, B, W, and R light curves from Wood *et al.* [29]. The solid curves

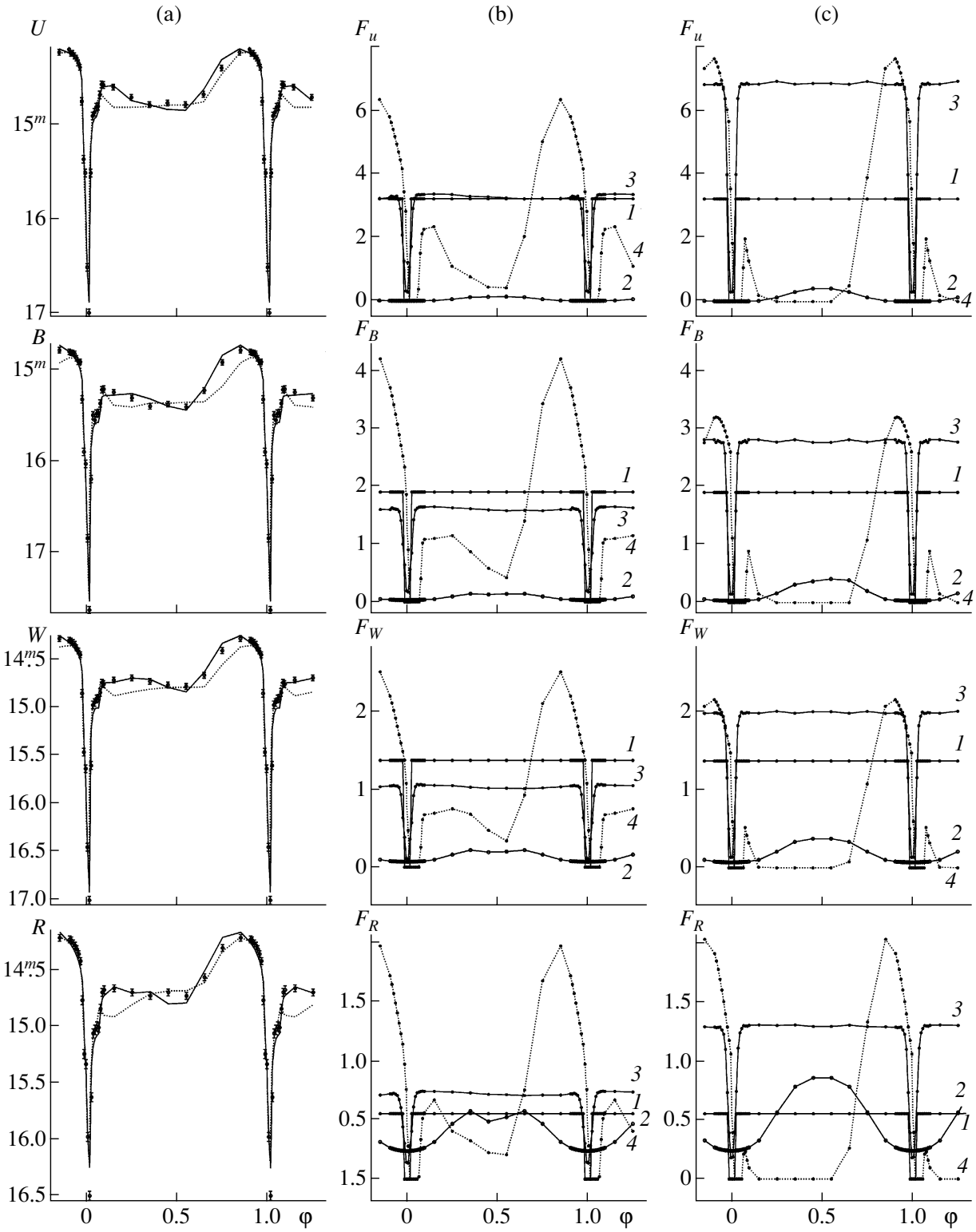

Fig. 4. Interpretation of the U, B, R, and white light (W) light curves of OY Car in the inactive state averaged over several orbital cycles, according to Wood *et al.* [29]. (a) Observations of [29] (points) and theoretical light curves synthesized for the hot-line (solid curves) and hot-spot (dashed curves) models. (b, c) Contributions to the total flux from the white dwarf (*1*), donor star (*2*), elliptical disk (*3*), and region of energy release (*4*) (hot line (b) or hot spot (c)). The flux is given in arbitrary units.

Table 3. Theoretical parameters of OY Car in its inactive state, derived from the U, B, W, R light curves of [29] averaged over several orbital cycles in the hot-line and hot-spot models

Parameter	U	B	W	R
Hot-line model				
Disk				
a/a_0	0.367(1)	0.361(1)	0.348(1)	0.350(1)
$a_{\max}/\xi$	0.596(1)	0.593(1)	0.577(1)	0.578(1)
e	0.164(2)	0.178(1)	0.188(1)	0.181(1)
α_e, deg	119(2)	129(2)	147(2)	136(3)
α_g	0.70(3)	0.68(3)	0.73(2)	0.74(1)
T_b, K	27 320(1000)	22 960(1200)	22 465(1100)	23 150(1050)
Hot line				
a_v/a_0	0.090(4)	0.055(3)	0.054(3)	0.069(4)
b_v/a_0	0.349(1)	0.326(1)	0.356(1)	0.384(2)
c_v/a_0	0.0276(1)	0.0192(1)	0.0182(1)	0.0214(1)
$T^{(1)}_{\max}$, K	13 543(2400)	16 680(2500)	15 615(2340)	15 140(2230)
$T^{(2)}_{\max}$, K	11 285(450)	12 655(400)	10 895(480)	11 375(540)
$\langle T^{(1)}\rangle$, K	7460	7615	6750	8090
$\langle T^{(2)}\rangle$, K	7245	6900	6235	7465
χ^2	168	207	186	204
Hot-spot model				
Disk				
r_d/a_0	0.278(1)	0.394(1)	0.284(1)	0.249(1)
r_d/ξ	0.388(1)	0.550(1)	0.397(1)	0.348(1)
T_b, K	30 740(1250)	26 380(1100)	24 940(1000)	25 825(1540)
Hot spot				
r_{sp}/a_0	0.095(5)	0.038(2)	0.057(4)	0.049(3)
α_{sp}, deg	40(6)	30(5)	43(6)	54(6)
T_{sp}	7130(220)	9300(150)	7510(200)	14 670(500)
χ^2	320	353	290	308

Note: The W light curve was obtained in white light ($\lambda_{\text{eff}} = 4960$ Å). The parameters of the disk and the region of energy release (hot line or hot spot) were obtained for fixed $q = M_1/M_2 = 9.8$, $i = 82°$, $T_2 = 3000$ K, $T_1 = 15\,000$ K, $R_1 = 0.0182a_0$. The maximum and minimum radii of the disk for the known e are determined from the formulas $a_{\max} = a(1+e)$ and $a_{\min} = a(1-e)$, where a is the semimajor axis of the disk. For all curves, the flaring angle of the outer edge of the disk is roughly the same in both models, $\beta_d = 3°.8–4°.1$, the parameter $y_{\min} = 0.28(2)a_0$, and the shift of the center of the hot region on the windward side of the line $\Delta y = 0.03(1)a_0$. In the hot-line model, $\alpha_g = 0.74(1)$ for all light curves.

show theoretical light curves synthesized for the hot-line model using the parameters from Table 3. Figure 4b presents the contributions of the white and red dwarfs, the disk, and the region of energy release (i.e., the hot line) to the total flux in the hot-line model in arbitrary units. It is clear that the red dwarf's contribution to the total flux in the blue (U and B) is negligible in this model ($< 2\%$). The contribution of the secondary increases to 3.5% in white light (W), and to 13.7% in R. The contribution from the

white dwarf is $\sim$24–25% in the blue and $\sim$30% in white light, decreasing to $\sim$16% in R. The maximum contribution from the disk is reached in U ($\sim$25%); in the other filters, it is $\sim$21–22% of the maximum flux from the system. The variations of the system's brightness at orbital phases $\varphi \sim 0.15$–0.85 are primarily determined by variations in the flux from the hot-line surface. It follows from Table 3 that the longitude of the disk periastron increases (by $\sim 30°$) in the transition from blue to red wavelengths. It is also possible that the different α_e in the red and blue are related to different contributions from components that were not taken into account in the model, such as the stream flowing out from the red dwarf, whose contribution increases in the red.

The lower part of Table 3 contains the results for the averaged light curves of OY Car obtained with the hot-spot model. Figure 4a (dashed curves) presents theoretical light curves synthesized in four filters for the best-fit parameters of the hot-spot model. Comparison of the theoretical curves indicates that the shape of the eclipse is described in a similar way in both models. The differences between out-of-eclipse portions of the light curves, particularly the shapes of the peak, are appreciably larger (Fig. 4a). In the hot-spot model, the contributions from the disk and white dwarf (Fig. 4c) are constant at phases $\varphi \sim 0.22$–0.67, the hot spot is not visible, and the model is unable to fit the observed light curves accurately. The contribution from the red dwarf is insignificant in the blue due to the low temperature and relatively small size of the star; as a result, the light curves display a flat portion at orbital phases $\varphi \sim 0.1$–0.6. In white light and R, the flux from the red dwarf becomes comparable to that from the white dwarf and disk, and determines the shape of the W and R light curves at phases $\varphi \sim 0.1$–0.6.

In the hot-line model, fluctuations of the out-of-eclipse flux are specified primarily by variations of the contribution from the shock. In all four filters, the contribution to the total flux from the shock front is fairly substantial (at the maximum, it is 25–35% of the radiation of the leeward side of the line), and it never becomes zero. Therefore, individual portions of the region of energy release are also visible at phases at which the hot spot cannot be seen. Due to the small eccentricity of the disk, the flux from the disk is constant at orbital phases at which it is not eclipsed by the red dwarf. The hot region at the edge of the stream in the vicinity of the accretion disk is not totally eclipsed in any of the considered portions of the light curve ($\varphi \sim 0.2$–0.7). At phases $\varphi \sim 0.1$–0.3, we see the radiation from the windward side of the hot line, from peripheral portions of the compact region heated by the shock. The hottest region is screened from the observer by the edge of the disk. Starting with phase $\varphi \sim 0.55$, we begin to see the radiation from the leeward side of the line in the hot-line model. Since the region of interaction is rather extended in this model, its projection onto the plane of the sky varies with orbital phase more smoothly than in the case of a quasiflat hot-spot surface, thus leading to the larger width of the orbital peak (cf. Figs. 4b, 4c).

5. INFRARED LIGHT CURVES OF OY Car

Sherrington *et al.* [21] obtained J (1.25 micron) observations of OY Car on April 25, 1980 and J and K (2.2 micron) observations on January 26, 1981. On April 25, 1980, OY Car was in its inactive state, while the system underwent a small flare in the J filter by $\sim 0\overset{m}{.}35$ on January 26, 1981. All the IR light curves display two pronounced minima during the orbital cycle, the shallower secondary minimum being at phase $\varphi \sim 0.5$. The depths of the primary minimum in the J light curves were $\sim 0\overset{m}{.}8$ in April 1980 and $\sim 1\overset{m}{.}0$ in January 1981 (they were $\sim 0\overset{m}{.}7$ in the K filter in the same period of time).

After removing the ellipsoidal curve for the variability of the secondary from the observed J light curves, Sherrington *et al.* [21] discovered that the secondary minimum essentially disappeared in the April J light curve, whereas it remained in the January J light curve (at the maximum of the small flare). The $J-K$ color index in the inactive state was $J-K = 0\overset{m}{.}93 \pm 0\overset{m}{.}15$; during the flare, it decreased to $J-K = 0\overset{m}{.}35 \pm 0\overset{m}{.}15$. The first value corresponds to a disk with a cool outer edge, while the second corresponds to a substantially hotter edge. The outer ring of the disk and the secondary make a substantial contribution to the system's flux at wavelengths $\lambda > 8000$ Å. The secondary alone contributes from 30 to 60% of the total IR flux, according to the estimates of [21].

We considered all three OY Car light curves presented by Sherrington *et al.* [21] in both the hot-line and hot-spot model. The observational data were taken from the plots presented in [21]. The April 25, 1980 J curve contains 330 individual observations, and the averaged curve 24 points; the January 26, 1981 J and K curves contain 405 and 108 observations, respectively, and the averaged curves 28 and 17 points. The rms errors of the averaged J curves are roughly equal: $\sigma \simeq 0\overset{m}{.}01$–$0\overset{m}{.}02$.

The K curve contains fewer observations and their scatter is higher; as a result, $\sigma \simeq 0\overset{m}{.}02$–$0\overset{m}{.}03$. A drift due to the small flare was subtracted from the J data for January 26, 1981 (no drift is seen in the K curve). The upper parts of Figs. 5 and 6 present the light curves used to derive the system parameters at IR wavelengths. The bars to the right of each plot

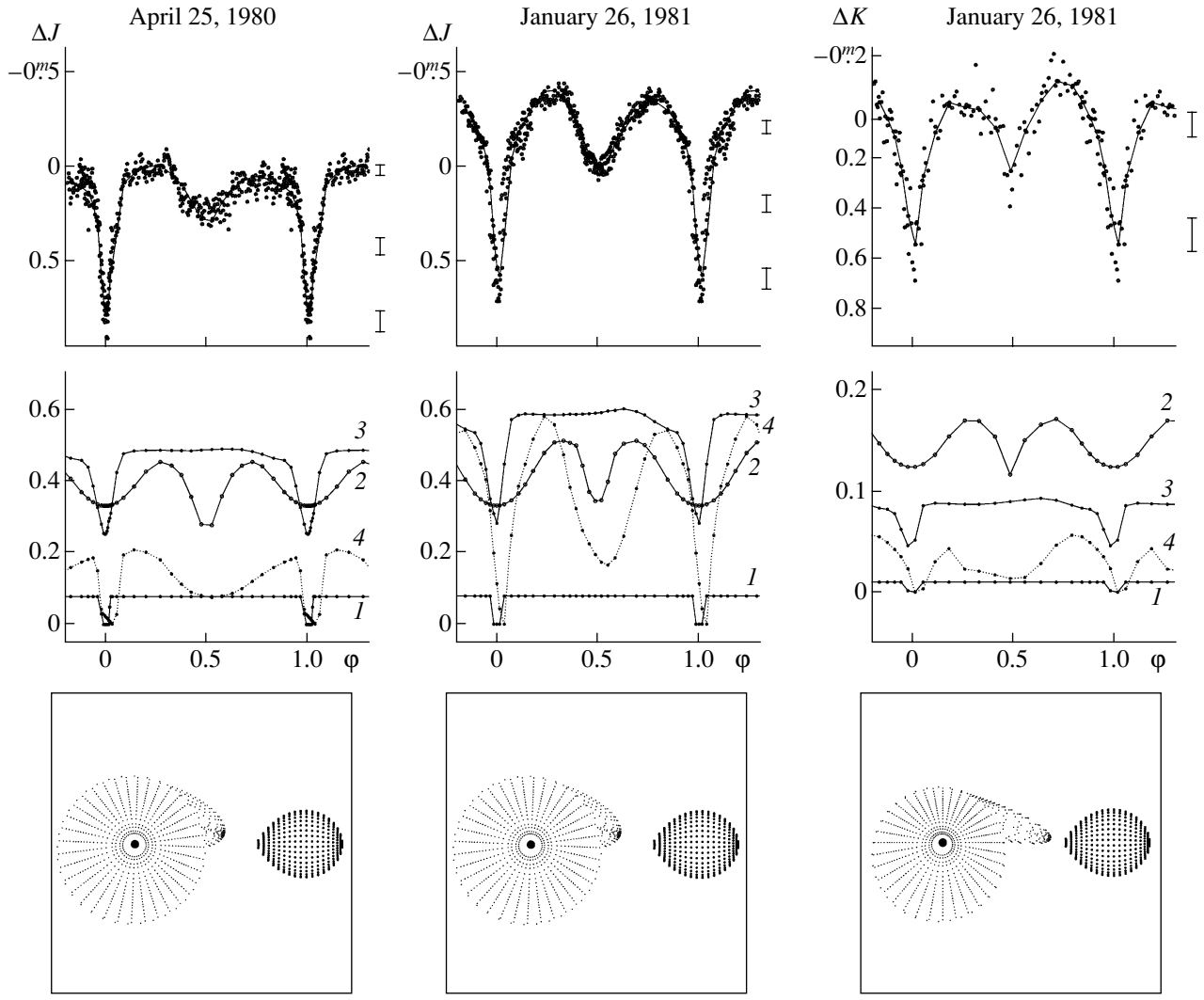

Fig. 5. Upper plots: the J and K observations of OY Car from Sherrington *et al.* [21] in the inactive state of the system on April 25, 1980 and during the small flare on January 26, 1981. The solid curves indicate the light curves synthesized in the hot-line model. The bars to the right of the plots indicate the mean errors of individual observations in the corresponding magnitude interval. The averaged plots present the contributions from various components to the total flux (in arbitrary units): the white dwarf (*1*), donor star (*2*), elliptical disk (*3*), and hot line (*4*). Lower plots: simulated images of OY Car (viewed from above) in the hot-line model, calculated with the parameters from Table 4.

indicate the mean error of the individual observations in the corresponding magnitude interval.

Both J light curves display a peculiar shape—the flux from the system before the ingress into the primary eclipse is slightly lower than immediately after the egress from the eclipse. In the hot-spot model, an additional source of radiation must be invoked to explain this.

To restrict the range of allowed system parameters in the IR, we took into account the homogeneity of both the J light curves. Both observed curves were shifted by $\delta J = 14.^m4$, which is the first-quadrature J flux obtained on April 25, 1980. Accordingly, we used the first-quadrature intensity corresponding to the best-fit parameters obtained for the J light curve of April 25, 1980 to translate the fluxes into magnitudes in the calculated trial theoretical light curves for both J light curves.

As for the B light curves of OY Car, the main system parameters were fixed using the values in Table 1. Table 4 presents the derived parameters of the disk and hot line. The maximum radius of the disk at near-IR wavelengths is roughly the same in the inactive state and during the weak flare ($a_{\max}/\xi \sim 0.67$–0.69). In the unperturbed state, the disk is almost circular, and the region of energy release is close to the edge of the disk and spans almost 60° in azimuth. The main contribution to the total flux (see the middle part of Fig. 5) is from the red dwarf,

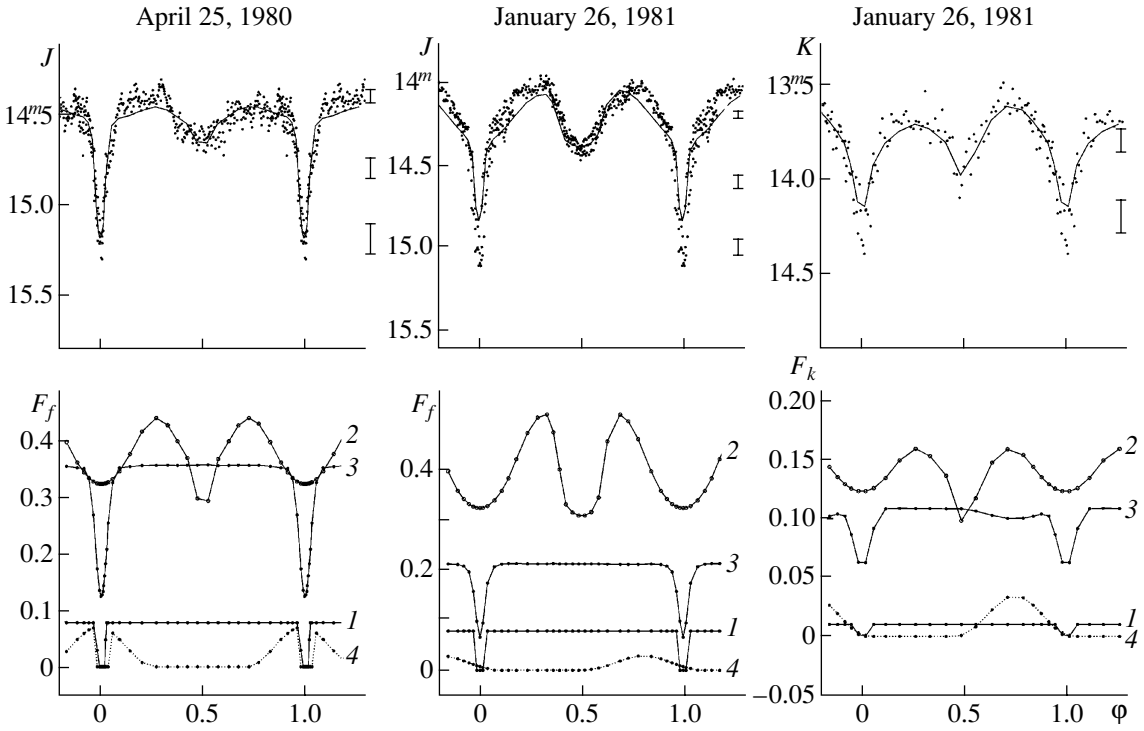

Fig. 6. Upper plots: the J and K observations of OY Car from Sherrington *et al.* [21] in the inactive state of the system on April 25, 1980 and during the small flare on January 26, 1981. The solid curves indicate the light curves synthesized with the best-fit parameters (Table 4) from the hot-spot model. Lower plots: the contributions from various components to the total flux (in arbitrary units): the white dwarf (*1*), donor star (*2*), elliptical disk (*3*), and hot spot (*4*).

whose polar areas are heated by hot radiation from the inner regions of the disk (from ∼30% to ∼54% of the total flux), and the disk (∼40% of the maximum total flux). The contribution of the white dwarf to the total flux is insignificant (about 6–8%). The contribution from the windward side of the hot line is slightly higher than from the leeward side—∼18% and ∼15%, respectively—resulting in the anomalous shape of the light curve. The brightness temperature of the hot line at the shock front reaches ∼40 000 K, which is not surprising, since the radiation has a recombination rather than blackbody origin. However, the size of this region is small, and the temperature falls very quickly to ∼3200 K with distance from the disk edge. As a result, the flux from this region is only 3% higher than the flux from the leeward side of the line, where the matter is heated on average to 3600 K, but the energy-release region spans almost 60° in azimuth. Since our assumption that the hot line emits a Planck spectrum is rather crude, the brightness temperature of the line should be considered a formal parameter.

During the small flare (see the bottom part of Fig. 5, where the comparative sizes of the disk and hot line are presented), a condensation is observed in the region of the disk close to the trajectory of the gaseous stream (formally, this is shown by the fact that the disk acquires the eccentricity $e \simeq 0.18$). In addition, the contribution from the hot line increases substantially (to 34% of the maximum flux), basically due to the increase in the size of the region of energy release. As in the inactive state, the contribution from the windward side of the line in the J filter is slightly higher (by ∼2%) than that from the leeward side, resulting in a slight asymmetry of the brightness maxima in the J light curve. Despite the fact that the absolute flux from the disk increases by ∼10% in this observational period, its relative contribution to the total flux decreases by ∼5–6% due to the increase of the flux from the hot line.

The parameters of the disk and hot line derived from the K light curve of OY Car (Table 4) are roughly the same. The increase of the brightness temperature of the hot line in the transition from the J to the K filter is apparently due to the deviation of the radiation from blackbody in this region and the contribution of free–free transitions to the observed radiation. As was noted in [12], where we analyzed light curves of the cataclysmic variable IP Peg, the hot-line radiation includes a substantial contribution from thermal bremsstrahlung and recombination radiation, whose fraction appreciably increases with increasing wavelength compared to the blackbody contribution.

Table 4. Theoretical parameters of OY Car in the IR derived from the light curves of [21]

Parameter	J	J	K
	April 25, 1980	January 26, 1981	January 26, 1981
Hot-line model			
a/a_0	0.440	0.401	0.374
$a_{\max}/\xi$	0.673	0.662	0.689
e	0.094	0.183	0.320
α_e, deg	57.46	70.00	82.00
α_g	0.508	0.586	0.629
T_b, K	16 265	21 395	20 945
a_v/a_0	0.183	0.111	0.064
b_v/a_0	0.424	0.562	0.515
c_v/a_0	0.013	0.022	0.015
$T^{(1)}_{\max}$, K	40 090	26 775	41 415
$T^{(2)}_{\max}$, K	4180	9635	12775
$\langle T^{(1)} \rangle$, K	19 290	13 575	13 100
$\langle T^{(2)} \rangle$, K	3660	6280	6175
$y_{\min}/a_0$	0.385	0.446	0.343
χ^2	197	205	10.8
Hot-spot model			
r_d/a_0	0.402	0.643	0.398
r_d/ξ	0.288	0.898	0.556
α_g	0.504	0.75	0.50
T_b, K	15 155	21 215	15 740
r_{sp}/a_0	0.025	0.365	0.134
α_{sp}, deg	4.79	69.30	87.01
T_{sp}, K	6750	4415	5300
χ^2	350	824	84.5

Note: The parameters of the disk and hot line (hot spot) were derived for fixed $q = M_1/M_2 = 9.8$, $i = 82°$, $T_2 = 3000$ K, $T_1 = 15\,000$ K, $R_1 = 0.0182a_0$. The flaring angle of the outer edge of the disk for all curves in both models is $\beta_d = 2°.5–3°.7$.

In the hot-spot model, the resulting residual for the J and K light curves ($\chi^2 \sim 350$, ~ 824 and 84.5 for the two J light curves and the K light curve, respectively; see Fig. 6, Table 4) is substantially higher than in the hot-line model ($\chi^2 \sim 194$, ~ 139 and 9.58, respectively). This is primarily due to the inconsistency between the observations and the theoretical depth of the primary minimum (for light curves obtained during the flare), as well as the flux near quadrature. In our model, the J light curves were analyzed independently in order to obtain the minimum residual. However, even in this approach, the derived azimuth of the hot spot does not coincide with the values calculated assuming the gaseous stream follows the ballistic trajectory for a particle ejected from the inner Lagrange point [29] for $q \simeq 10.0$ and that the hot spot should be located at the point where the ballistic trajectory intersects the edge of the disk ($\alpha_{sp} \sim 32°–36°$). Finally, as expected, this model is unable to describe the anomalous shape of the J light curves, in both the inactive state and during the flare.

6. CONCLUSION

Our interpretation of eclipsing light curves of the cataclysmic variable OY Car using two alternative models indicates that the hot-line model describes the observed light curves in the inactive state of the system substantially better than the hot-spot model. The hot-line model better reproduces the width of the peaks in the light curves, the shape of the eclipse, and the details of out-of-eclipse brightness variations. The hot-spot model for a system with a very high component mass ratio is unable to describe the out-of-eclipse brightness variations in the optical orbital curves. In this case, the contribution from the radiation of the red dwarf is negligible, the out-of-eclipse fluxes from the disk and the white dwarf are constant, and the only source of out-of-eclipse variations is the hot spot at phases 0.7–0.9. Due to the possibility of varying the parameters of the shock—the temperature and size of the region of energy release—and also due to the location of the energy-release region outside the disk, the hot-line model is able to reproduce the shape of out-of-eclipse portions of the light curves for this SU UMa-type system, which can vary in the transition from one orbital cycle to another. Unlike the hot spot, relatively bright regions of the hot line can also be observed at phases $\varphi \sim 0.5$–0.6, when the hot spot at the point of contact between the stream from L_1 and the disk is not visible. Finally, with an appropriate orientation of the elliptical accretion disk, an increase of the flux from the system at phases $\varphi \sim 0.1$–0.2 will be observed due to the radiation from the windward side of the hot line, which is completely ruled out in terms of the standard model.

The advantages of the hot-line model over the hot-spot model are manifest in each of the 20 individual B light curves of OY Car in the quiescent state, in spite of the substantial variations of these light curves from period to period. In all 20 individual curves, we can see the trend for an increase of the flux in the primary minimum with increasing luminosity of the accretion disk. The flux at the maximum of the orbital peak increases linearly with the increase of the total contribution from the disk and hot line.

Our analysis of IR light curves of OY Car confirms the advantages of the hot-line model, which can explain the anomalous IR light curves of this system in a natural way.

7. ACKNOWLEDGMENTS

This work was supported by the Russian Foundation for Basic Research (project nos. 02-02-16462, 02-02-17524, 02-02-16088), the INTAS Foundation (grant no. 00-491), the State Science and Technology Project "Astronomy," Presidential Grants of the Russian Federation (00-15-96722, 00-15-99311), and the State Science and Technology Project "Universities of Russia" (grant 5558).

REFERENCES

1. V. G. Gorbatskiĭ, Astrofizika **3**, 245 (1967).
2. J. Smak, Acta Astron. **20**, 312 (1970).
3. B. Warner, *Cataclysmic Variable Stars* (Cambridge Univ. Press, Cambridge, 1995).
4. D. V. Bisikalo, A. A. Boyarchuk, O. A. Kuznetsov, and B. M. Chechetkin, Astron. Zh. **74**, 880 (1997) [Astron. Rep. **41**, 786 (1997)].
5. D. V. Bisikalo, A. A. Boyarchuk, O. A. Kuznetsov, and B. M. Chechetkin, Astron. Zh. **74**, 889 (1997) [Astron. Rep. **41**, 794 (1997)].
6. D. V. Bisikalo, A. A. Boyarchuk, V. M. Chechetkin, *et al.*, Mon. Not. R. Astron. Soc. **300**, 39 (1998).
7. D. V. Bisikalo, A. A. Boyarchuk, O. A. Kuznetsov, *et al.*, Astron. Zh. **75**, 706 (1998) [Astron. Rep. **42**, 621 (1998)].
8. D. V. Bisikalo, A. A. Boyarchuk, B. M. Chechetkin, *et al.*, Astron. Zh. **76**, 905 (1999) [Astron. Rep. **43**, 797 (1999)].
9. D. V. Bisikalo, A. A. Boyarchuk, B. M. Chechetkin, and O. A. Kuznetsov, Astron. Zh. **77**, 31 (2000) [Astron. Rep. **44**, 26 (2000)].
10. M. Makita, K. Miyawaki, and T. Matsuda, Mon. Not. R. Astron. Soc. **316**, 906 (2000).
11. D. V. Bisikalo, A. A. Boyarchuk, O. A. Kuznetsov, *et al.*, Astron. Zh. **75**, 40 (1998) [Astron. Rep. **42**, 33 (1998)].
12. T. S. Khruzina, A. M. Cherepashchuk, D. V. Bisikalo, *et al.*, Astron. Zh. **78**, 625 (2001) [Astron. Rep. **45**, 538 (2001)].
13. C. Hoffmeister, Veroff. Sternwarte Sonneberg **6** (1), 5 (1963).
14. N. Vogt, R. Schoembs, W. Krzeminski, and H. Pedersen, Astron. Astrophys. **94**, L29 (1981).
15. N. Vogt, Astron. Astrophys. **128**, 29 (1983).
16. R. Schoembs and K. Hartmann, Astron. Astrophys. **128**, 37 (1983).
17. R. Schoembs, H. Dreier, and H. Barwig, Astron. Astrophys. **181**, 50 (1987).
18. M. C. Cook, Mon. Not. R. Astron. Soc. **215**, 211 (1985).
19. G. Berriman, Mon. Not. R. Astron. Soc. **207**, 783 (1984).
20. G. Berriman, Mon. Not. R. Astron. Soc. **210**, 223 (1984).
21. M. R. Sherrington, R. F. Jameson, J. Bailey, and A. B. Giles, Mon. Not. R. Astron. Soc. **200**, 861 (1982).
22. J. Bailey and M. Ward, Mon. Not. R. Astron. Soc. **194**, 17P (1981).
23. K. V. Hessman, D. Koester, R. Schoembs, and H. Barwig, Astron. Astrophys. **213**, 167 (1989).
24. E. T. Harlaftis and T. R. Marsh, Astron. Astrophys. **308**, 97 (1996).
25. W. Krzeminski and N. Vogt, Astron. Astrophys. **144**, 124 (1985).
26. R. Schoembs, Astron. Astrophys. **158**, 233 (1986).
27. A. Bruch, D. Beele, and R. Baptista, Astron. Astrophys. **306**, 151 (1996).
28. G. Berriman, Mon. Not. R. Astron. Soc. **228**, 729 (1987).

29. J. H. Wood, K. Horne, G. Berriman, and R. A. Wade, Astrophys. J. **341**, 974 (1989).
30. T. Hamada and E. E. Salpeter, Astrophys. J. **134**, 683 (1961).
31. J. Smak, Acta Astron. **34**, 317 (1985).
32. T. S. Khruzina, Astron. Zh. **78**, 298 (2001) [Astron. Rep. **45**, 255 (2001)].
33. T. S. Khruzina, Astron. Zh. **75**, 209 (1998) [Astron. Rep. **42**, 180 (1998)].
34. K. V. Hessman, K.-H. Mantel, H. Barwig, and R. Schoembs, Astron. Astrophys. **263**, 147 (1992).
35. O. A. Kuznetsov, D. V. Bisikalo, A. A. Boyarchuk, *et al.*, Astron. Zh. **78**, 997 (2001) [Astron. Rep. **45**, 872 (2001)].

Translated by K. Maslennikov